JOURNAL OF GEOPHYSICAL RESEARCH, VOL. 105, NO. E2, PAGES 4153–4164, FEBRUARY 25, 2000

Long-wavelength topographic relaxation for self-gravitating planets and implications for the time-dependent compensation of surface topography

Shijie Zhong and Maria T. Zuber

Department of Earth, Atmospheric and Planetary Sciences, Massachusetts Institute of Technology, Cambridge

Abstract. The support of planetary surface topography is controlled by the thickness of the elastic lithosphere and thus has implications for the thermomechanical structure of shallow planetary interiors. Previous analyses of the support of long-wavelength topography have generally utilized elastic formulations, which preclude consideration of the time evolution of lithospheric stresses and thermal state. Here we formulate a viscoelastic model for the support of topography on a spherical planet. Our stress relaxation model employs a multilayer linear viscoelastic rheology and includes the effect of self-gravitation. In these models we approximate internal rheology with an olivine flow law, and we estimate the internal thermal structure assuming simple conductive cooling. We analyze how relief at the surface and internal density interfaces evolves with time in response to a surface or internal load. Our analysis demonstrates that crustal compensation is strongly dependent on planetary radius, with a tendency for a large terrestrial planet like Earth to reach complete Airy isostasy at long wavelengths within a time scale controlled by the mantle viscosity. The correlation of degree of compensation with planetary radius is consistent with previous work [*Turcotte et al.*, 1981], which showed that membrane stress can support significant long-wavelength gravity anomalies. Applied to the Moon, the degree of compensation associated with loading of 100-Ma lithosphere is less than 0.3, and the load Love numbers are greater than -0.6 for all harmonics including degree 2, even after 10^9 years of relaxation. This conclusion does not change significantly even with a moderately low viscosity for the crust. The tendency for a small body like the Moon to support long wavelength stresses may be relevant in understanding the anomalously large degree 2 terms in the lunar shape. The results also suggest that major impact basins would not be compensated throughout lunar geological history (> 4 b.y.), even if the surfaces on which the basins were initially formed were relatively young (i.e., 100 – 300 Ma). The fact that the South Pole-Aitken basin is largely compensated suggests that the lateral variations in thermal and/or mechanical structure induced by impact processes play significant roles in the compensation of this structure.

1. Introduction

The topography [*Turcotte*, 1987] and gravity [*Phillips and Lambeck*, 1980] fields of the terrestrial planets have significant power at long wavelengths. Depending on the thermal and mechanical structure of planetary interiors, the long-wavelength anomalies can be supported either statically by the rigid surface layer (i.e., lithosphere) or dynamically through planetary mantle convection [e.g., *Turcotte et al.*, 1981; *Hager and Richards*, 1989]. Long-wavelength anomalies may provide important constraints on the structure and dynamics of the interiors. On the Moon and Mars, large positive gravity anomalies (also known as mascons) are associated with major impact basins [*Mueller and Sjogren*, 1968; G.L. Tyler, personal communication, 1999]. Analysis of gravity and topography signatures of major lunar basins indicates that their degree of compensation is variable [*Zuber et al.*, 1994; *Neumann et al.*, 1996]. While the South Pole-Aitken basin, the largest and oldest lunar basin, is almost fully compensated, other younger and smaller basins deviate from compensation to various extents [*Neumann et al.*, 1996].

Studies of the response of thin elastic shells to surface or subsurface loads [*Turcotte et. al.*, 1981; *Willemann and Turcotte*, 1981] indicate that a planet with a strong lithosphere can support significant deviatoric stresses at the longest wavelengths (up to degree 2). *Turcotte et al.* [1981] demonstrated that the ability to support long-wavelength deviatoric stresses increases with decreasing planetary radius and increasing elastic shell thickness. The sensitivity of compensation state on planetary radius has been recognized to be a membrane stress effect by *Turcotte et al.* [1981], who suggested that the long-wavelength gravity anomalies on the Moon and Mars are supported by the elastic strength of the lithosphere. The capacity of the planetary surface layer to support deviatoric stresses also has important implications for understanding convection-driven gravity anomalies. In studies of the Earth's long-wavelength geoid, elastic support of loads has often been ignored because the effect is relatively small [*Hager and Richards*, 1989].

While these classic elastic shell models provide useful physical insights, they are oversimplified in three important aspects. First, planetary mechanical structure is more complicated than assumed in elastic models, which typically

Paper number 1999JE001075.
0148-0227/00/1999JE001075$09.00

consist of a thin shell of uniform rigidity that overlies an inviscid fluid sphere. Because the rheology for silicate planets is thermally activated [*Karato and Wu,* 1993], the radial stratification of lithospheric strength or viscosity is likely a quasi-continuous function of depth. However, for the Moon and other planets the uppermost layer may be significantly weaker than the underlying layers due to the pressure dependence of frictional strength, as well as processes such as impact cratering that results in comminution of shallow rock layers. Second, elastic shell models do not contain a time scale, which may be important in understanding the origin of different compensation states for surface structures with different ages. Thus the elastic formulations also preclude analysis of the evolution of compensation with time and do not allow lithosphere thickness to be easily factored into thermal evolution scenarios. Third, thin elastic shell models do not allow for the vertical variations of stress, which is a good approximation only when the shell thickness is much smaller than the horizontal dimension of the load [*Brotchie and Silvester,* 1969; *Brotchie,* 1971; *Turcotte and Schubert,* 1982]. Application of such a model to a small planetary body like the Moon with large elastic plate thickness may or may not be warranted. Consideration of these collective issues has motivated us to formulate more complete models of stress relaxation that include approximately continuous variations in lithospheric and mantle viscosities and elastic parameters. Our physical models are similar to those employed in the studies of postglacial rebound [e.g., *Cathles,* 1975; *Peltier,* 1976], though we are generally interested in longer-term stress relaxation within a planetary body than has been treated in the glacial loading studies. Our models also include a crust-mantle density interface that allows us to examine the dynamics of crustal compensation in association with the relaxation of surface or internal loads [*Zhong,* 1997].

In this paper we will investigate how surface and internal interface topography and stresses evolve with time in response to a surface or internal load for a self-gravitating planet with depth-dependent viscoelastic rheology. We will demonstrate that the relaxation time for long-wavelength topography is highly sensitive to planetary radius. For a planet with the radius of the Moon, even if the long-wavelength topographic anomalies initially formed on a young, relatively weak surface, more than 60% of the anomalies can be supported over the geological history of the Moon. In the following sections we will first present the mathematical formulation of our models and the solution approaches for solving the stress relaxation problems. Second, we will demonstrate that the thin elastic shell models are special cases of our viscoelastic models. Finally, we will show how stress relaxation and compensation depend on rheological parameters and planetary radius, and discuss the implications of our results.

2. Physical Models and Mathematical Formulation

2.1. Governing Equations

The response of a self-gravitating planet with incompressible viscoelastic rheology to stress loads can be described by the governing equations of mass and momentum and the equation of gravitational perturbation:

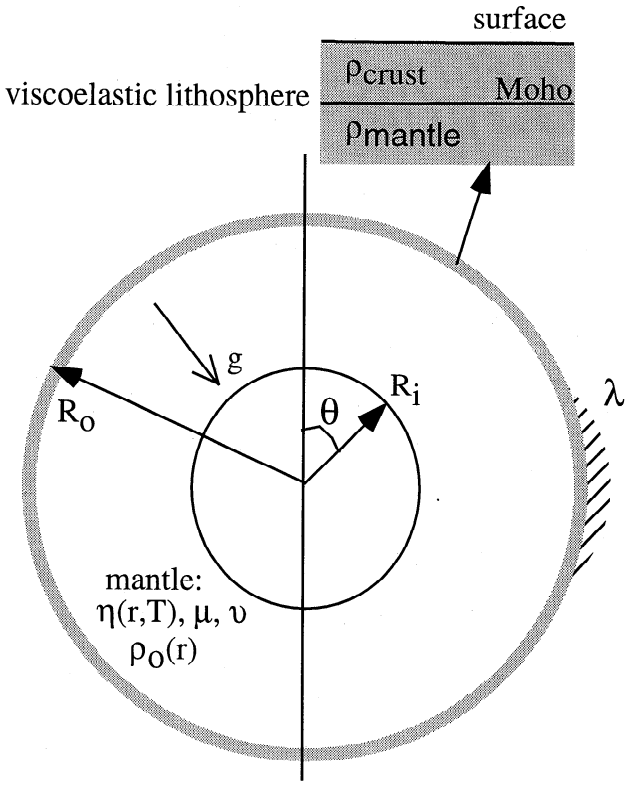

Figure 1. Schematic of the viscoelastic relaxation problem in spherical geometry. Both the mantle and crust are treated as viscoelastic media. Because superposition of spherical shells is allowed by our approach, the lithosphere may consist of a crust and upper mantle with distinctive mechanical properties. The viscosity for both the mantle and crust is described by a temperature- and depth-dependent Newtonian rheology $\eta(R,T)$. The model includes the effect of self-gravitation.

$$u_{i,i} = 0, \tag{1}$$

$$\sigma_{ij,j} + \rho_0 \phi_{,i} - \Delta\rho g \delta_{ir} = 0, \tag{2}$$

$$\phi_{,ii} = 4\pi G \Delta\rho, \tag{3}$$

where u_i is the velocity; σ_{ij} is the stress tensor; ρ_0 is a reference density that can be a function of r; ϕ is the perturbation of gravitational potential; g is the gravity acceleration; $\Delta\rho$ is the density perturbation, and δ_{ir} is the Kronecker delta, which equals 1 when $i=r$ and equals 0 otherwise (Figure 1). The rheological equation for an incompressible viscoelastic medium (i.e., Maxwell body) can be written

$$\sigma_{ij} + \frac{\eta}{\mu}\dot{\sigma}_{ij} = -P\delta_{ij} + 2\eta\dot{\varepsilon}_{ij}, \tag{4}$$

where μ and η are the shear modulus and viscosity, respectively; P is the pressure; ε is the strain tensor; and the dot over the strain and stress tensors denotes the time derivative.

For a given set of mechanical properties, manifest in our formulation by multiple layers with specified material constants, and a given surface or internal stress load, we will analytically solve the above equations for the time evolution

of stresses and surface topography at density interfaces in a spherical shell geometry. By assuming that viscoelastic properties within each layer are uniform and time-invariant, we can use a propagator matrix method to solve the equations, as is done for elastic displacement or pure viscous flow problems [e.g., *Hager and O'Connell,* 1981]. However, in our formulation, special treatment will be required to account for the nature of symbolic solutions in a Laplacian space [*Zhong,* 1997]. By solving equations (1) – (4) with multiple-layer viscoelastic structure and free surface boundary conditions (see Appendices A, B, and C for solution approaches), we can obtain solutions for the time evolution of interface relief at the surface, crust-mantle interface (i.e., Moho), and core-mantle boundary (CMB) for a given initial relief at any of these density interfaces. These equations could alternatively be solved by using the elastic solution and a correspondence principle as in postglacial rebound problems [*Peltier,* 1974].

In addition to tracking the time evolution of relief on density interfaces, we will use the degree of compensation [*Turcotte et. al.,* 1981] and load Love numbers [*Munk and MacDonald,* 1960; *Lambeck,* 1980] to measure the planetary response to loading. Since the response for a viscoelastic body is necessarily time-dependent, these parameters must also be time-dependent [*Mitrovica and Peltier,* 1992]. For each spherical harmonic degree l, the degree of compensation $D_c(l, t)$ and load Love number $k_L(l, t)$ at any given time t are given by

$$D_c(l,t) = -\frac{F_m(l,t)(\rho_m - \rho_{cr})}{F_s(l,t)\rho_{cr}}, \tag{5}$$

$$\phi_s(l,t) = [1 + k_L(l,t)]\phi_s^0(l), \tag{6}$$

where $F_s(l, t)$ and $F_m(l, t)$ are the topography at the surface and Moho, respectively; ρ_{cr} and ρ_m are the crustal and mantle densities, respectively; $\phi_s^0(l)$ is the initial surface gravitational potential that results from initial perturbed surface topography; and $\phi_s(l,t)$ is the surface potential at time t, which includes contributions from relief at the surface, Moho, and CMB (see equation (B7) in Appendix B).

2.2. Viscoelastic Properties

The Earth and the Moon are the only two planets for which elastic properties have been measured by seismology. To the first order, the elastic characteristics of both of these bodies can be characterized as radially stratified, but with considerable variation [*Toksoz et al.,* 1974; *Dziewonski and Anderson,* 1981; *Su and Dziewonski,* 1996; *Kennett et al.,* 1998]. We assume that the elastic parameters within a given layer are homogeneous. Compared with elastic properties, which provide an indication of the instantaneous response to loading, the long-term mechanical behavior (or effective viscosity) of planetary interiors is not well constrained. For Earth, studies of the postglacial rebound and long-wavelength geoid anomalies suggest that the average mantle viscosity is about 10^{21} Pa s, and the lower mantle may be a factor of 30 to 100 more viscous than the upper mantle [*Hager and Richards,* 1989; *Mitrovica and Forte,* 1997]. For the Moon, early estimates of the viscosity based on modeling the relaxation of lunar basins suggested that the viscosity in the upper 800 km of the Moon is about 10^{26} Pa s [*Arkani-Hamad,* 1973a], but we shall later show that such a high value is not required to support basin topography.

Laboratory studies on terrestrial silicate rocks suggest that mantle rheology depends primarily on the temperature, stress, and grain size, with the temperature dependence likely the most important [*Karato and Wu,* 1993; *Ranalli,* 1995]. The flow law for olivine rocks can be described as

$$\dot{\varepsilon} = A\left(\frac{\sigma}{\mu}\right)^n \left(\frac{d}{b}\right)^m \exp\left[-\frac{(E+PV)}{RT}\right], \tag{7}$$

where A is the preexponential frequency factor; μ is the shear modulus; d is grain size; b is the length of Burger's vector; n is the stress exponent; m is the grain size exponent; R is the gas constant; T is the temperature; E is the activation energy; P is the pressure; and V is the activation volume. From (7), we can define an effective viscosity

$$\eta = \frac{\sigma}{2\dot{\varepsilon}} = \eta_0 \exp\left[\frac{E+PV}{RT}\right], \tag{8}$$

where η_0 is a reference viscosity that includes the dependence of viscosity on stress and grain size as indicated in (7). We model the temperature dependence with multiple stacked constant viscosity layers. In our rheological equation we will use values of the activation energy and activation volume that are consistent with laboratory studies on terrestrial silicate rocks. For a specified rheology the viscosity structure can be constructed from a given radial temperature structure that we may approximate by assuming a certain surface age and a simple conductive (e.g., a half-space) cooling model.

Note that in this formulation we do not have the ability to treat a nonlinear stress-dependent rheology. However, for exponents in the range $3 \le n \le 5$, which is appropriate for silicate rocks, the stress dependence of rheology should not significantly affect our results. It is quite conceivable that planets with complex evolutionary histories may have variable rheologies, but it would be difficult to quantify the effects of such complexities on stress relaxation. In spite of these approximations, we believe that our models can yield some important first-order understanding regarding the nature of the relaxation of long-wavelength stresses on the terrestrial planets.

3. Results and Discussion

3.1. Comparison With Thin Elastic Shell Models

Brotchie and Silvester [1969] and *Brotchie* [1971] derived analytic solutions for deformation of a thin elastic shell with a disk load. Requirements for the use of thin shell theory include the following: (1) the shell is thin compared to its radius, (2) deflections are small compared to the shell radius, and (3) the variations of normal stresses in the radial direction are negligible. Thin spherical shell solutions have been used to study the instantaneous lithospheric response to large surface loads like mare filling of lunar impact basins [e.g. *Solomon and Head,* 1979] and volcanoes on Mars [*Comer et al.,* 1985] and Venus [*Banerdt,* 1986]. *Turcotte et al.* [1981] and *Willemann and Turcotte* [1982] adapted the theory of *Kraus* [1967] to investigate planet-scale loads by including additional bending terms and self-gravitation effects. Their formulation did not account for horizontal tractions due to topographic gradients [*Artyushkov,* 1973]. The solutions by

Turcotte et al. [1981] are based on a spherical harmonic analysis (i.e., spectral method), and the response of a thin elastic shell is given in terms of the degree of compensation for each harmonic. *Sleep and Phillips* [1985] also applied the theory of *Kraus* [1967] in a formulation that included only the membrane stress effect; their objective was to study the stress state of Mars due to loading associated with the Tharsis province.

A limited number of thick shell formulations have also been applied to global-scale problems in planetary tectonics. *Banerdt et al.* [1982] used such an approach to study the compensation of the Tharsis province, Mars, by performing a full integration of the elastic equations in spherical geometry [cf. *Arkani-Hamed,* 1973b], modified to include a laterally variable density interface at depth [*Kaula,* 1968]. The solution worked well for the longest planetary wavelengths but was unstable at high harmonic degrees. *Janes and Melosh* [1990] developed an analytical version of the thick shell theory for axisymmetric loads on a spherical elastic shell and explored the stress states and tectonic styles associated with ranges of load width and shell thickness.

We wish to verify our time-dependent solution in the limit of an elastic spherical shell over an inviscid fluid sphere. To accomplish this, we compare some viscoelastic solutions to those determined from thin shell elastic theory for the relaxation of an idealized basin. The calculation consists of three steps. First, we decompose the disk load into a spectral domain with 360 spherical harmonics. Then for each harmonic we compute the viscoelastic response using the approach described in the previous sections, but without self-gravitation because it was absent in the previous model [*Brotchie and Silvester,* 1969; *Brotchie,* 1971]. Finally, we compute the surface deflection from the summation of responses at different harmonics.

Table 1. Parameters for the Two-Layer Models

Parameter	Value
Shear modulus	5×10^{10} Pa
Poisson's ratio	0.5
Crustal density	2800 kg m^{-3}
Mantle density	3330 kg m^{-3}
Mean mantle density *	5515 kg m^{-3}
Core density†	7667 kg m^{-3}
Crustal thickness†	20 km
Outer radius	6370 km
Inner radius (CMB)†	3480 km
Gravitational acceleration (surface)	9.8 m s^{-2}
Viscosity of top layer†	10^{30} Pa s
Viscosity of bottom layer†	10^{21} Pa s

* Parameters used for the elastic shell calculations by *Turcotte et al.*, [1981] in addition to those unmarked parameters for the elastic shell models by *Brotchie* [1971].

†Additional parameters used for our viscoelastic calculations; the mean mantle density is not needed.

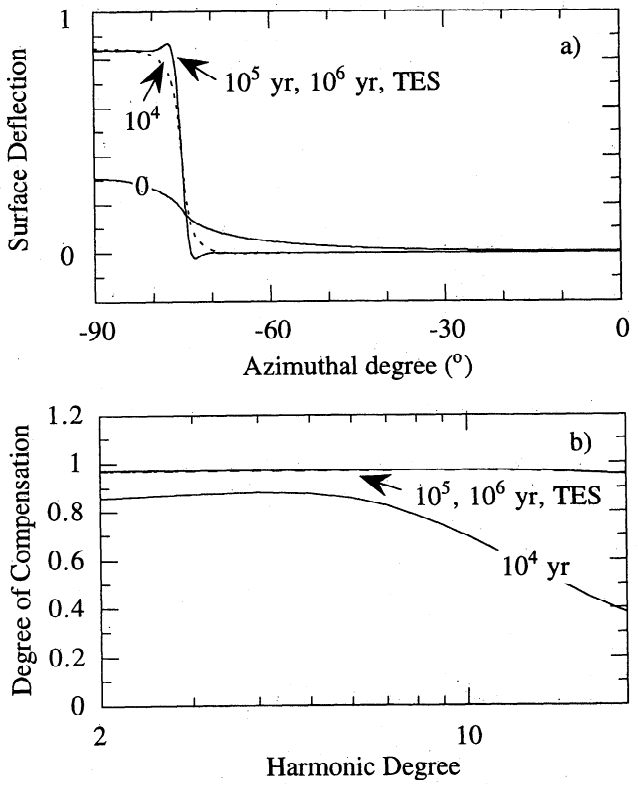

Figure 2. (a) Time evolution of surface deflection in response to a disk load for a viscoelastic model and the static response of a thin elastic shell (TES) to the same load. For this calculation, $\mu=5\times10^{10}$ Pa and the acceleration of gravity g= 9.8 m s^{-2}. (b) Time evolution of degree of compensation for harmonic degrees 2 to 20 for the viscoelastic model and degree of compensation for the thin elastic shell model.

For a basin-shaped load with an azimuthal radius of 15° and a unit depth on a 40-km-thick elastic shell with an outer radius of 6370 km (comparable to that of Earth), the surface deflection from the classical elastic shell model [*Brotchie and Silvester,* 1969; *Brotchie,* 1971; *Comer et al.,* 1985] is given in Figure 2a. The response to the same load from our viscoelastic model is necessarily time-dependent (Figure 2a). To compare with the elastic shell model, our viscoelastic model includes two layers with different viscosities: the top 40-km thick layer and an underlying layer extending to CMB at a radius of 3480 km, whose viscosities are 10^{30} Pa s and 10^{21} Pa s, respectively. The Moho is assumed to occur at a depth of 20 km (Table 1).

The response at $t=0$ represents the initial elastic response to the basin load, and this initial uplift at the basin center on the Moho is about 30% of the initial basin depth (Figure 2a). The deflection of the Moho increases with time, as the stresses within the weak mantle relax (Figure 2a). At about 10^5 years after loading, the deformation approximately reaches a steady state and remains unchanged over a long period of time (Figure 2a). The steady state deformation is nearly identical to that from the thin elastic shell calculation (Figure 2a). Clearly, the time that it takes to reach the steady state in the viscoelastic calculation is controlled by the viscosity in the bottom layer, as has long been recognized in postglacial rebound studies [e.g., *Peltier,* 1974; *Cathles,* 1975].

In order to examine the conditions under which our viscoelastic models begin to deviate from elastic spherical shell solutions [*Brotchie and Silvester,* 1969; *Comer et al.,* 1985], we have also made comparisons for different elastic plate thickness and load radii. For the viscoelastic models, we use only the steady state solutions. Figure 3a shows the results from the models with different load radii (15°, 30°, 60°,

and 90°) but the same mechanical properties as in Table 1. We observe that the steady state solutions from our viscoelastic models are in excellent agreement with those from the thin elastic shell model, even for load radii as great as 90°. This result is interesting given the common concern of the applicability of the elastic shell models for large disk loads [e.g., *Comer et. al.,* 1985].

As the elastic plate thickness T_e increases, we would expect the thin elastic plate assumption to eventually break down [cf. *Comer,* 1983]. For a fixed load radius of 30°, we compute thin elastic shell models with different thicknesses (T_e = 40 km, 80 km, 160 km, 320 km, and 640 km or T_e/R_o = 0.00628, 0.01256, 0.02512, 0.05024, and 0.10048) and compare them with the corresponding viscoelastic models. Other parameters are the same as in Table 1. Because the approximations made in the thin elastic shell models are wavelength-dependent, we perform the comparison in the spectral domain. For the same reason we also decompose the Brotchie solution into spherical harmonics. Figure 3b shows that the relative differences between the elastic shell solution and our viscoelastic models increase with increasing shell thickness. The spikes in the relative differences that occur first at l=7 and then at every 6 harmonics are caused by the use of a disk load in the models, with the spacing of the spikes controlled by the load radius (i.e., 30°). However, the gradual trend in the relative differences does not depend on load radius. We observe from the gradual trend that the difference between these two models is less than 5% as long as the wavelength is more than 5 times greater than the elastic plate thickness for T_e/R_o as large as 0.1 (Figure 3b). This result indicates that the thin elastic shell model represents a good approximation under these conditions. However, the conclusion depends on planetary radius. We find that when T_e/R_o and other parameters are fixed, the relative difference increases at long wavelengths with decreasing planetary radius. This difference is greater if the effect of reduced gravity for small planets is considered (Fig. 3c). Figure 3c also demonstrates that the relative difference at short wavelengths does not depend on the planetary radius.

Turcotte et al. [1981] considered the effects of self-gravitation in thin elastic plate models because this effect is important at long wavelengths. These workers presented degree of compensation (D_c) for different spherical harmonics. In their thin elastic shell formulation the mean density for a planet is needed, and it is taken as 5515 kg m^{-3}, the mean density for the Earth. With the same model parameters as in Table 1, D_c for harmonic degrees from 2 to 20 is shown in Figure 2b. The compensation parameter, D_c, for our viscoelastic model with the self-gravitation is time-dependent. However, after 10^5 years, D_c reaches the steady state and is identical to that from *Turcotte et al.* [1981]. The value of D_c is very close to unity for degrees 2 to 20, which indicates that the surface loads are nearly isostatically compensated for this model (Figure 2b). However, it is interesting that D_c is not exactly equal to unity even at degree 2.

3.2. Effect of Planetary Radius on Relaxation

Using their thin elastic shell models, *Turcotte et al.* [1981] and *Willemann and Turcotte* [1981] indicated that due to membrane stresses, planetary radius has a significant influence on the capability of planetary lithosphere to support deviatoric stresses (i.e., topography). They suggested that for planets like Mars and the Moon, gravity anomalies are mainly supported by the lithosphere even at the longest wavelengths, including degree 2. We now address the role of planetary radius in crustal compensation with our viscoelastic models.

Table 2. Model Parameters for Viscoelastic Models With Multiple Layers*

Parameter	Value
Activation energy (wet, dry)	(240, 300) KJ mol^{-1}
Activation volume	5x10^{-6} m^3 mol^{-1}
Maximum viscosity	10^{30} Pa s
Reference viscosity	10^{19} Pa s
Earth	
Core density	7667 kg m^{-3}
Crustal thickness	20 km
Outer radius	6370 km
Inner radius (CMB)	3480 km
Gravitational acceleration (surface)	9.8 m s^{-2}
Mars	
Core density†	6600 kg m^{-3}
Crustal thickness†	40 km
Outer radius	3398 km
Inner radius (CMB)†	1000 km
Gravitational acceleration (surface)	3.72 m s^{-2}
Moon	
Core density†	6600 kg m^{-3}
Crustal thickness	60 km
Outer Radius	1740 km
Inner radius (CMB)†	300 km
Gravitational acceleration (surface)	1.63 m s^{-2}

*Elastic parameters, crustal and mantle densities are the same as in Table 1.
†The choices of these parameters are arbitrary, but do not affect the model results.

First, we compute three cases for hypothetical planets that have different radii: 2000 km, 3000 km, and 6000 km. These three calculations are designed to isolate the effects of planetary radius on crustal compensation. The gravitational acceleration is assumed to be linearly proportional to the planetary radius (i.e., constant planetary density), and self-gravitational effects are included. The radius of the core-mantle boundary is taken to be 500 km. We will use multiple layers to represent a continuous viscosity structure that is derived from a thermally activated rheology for dry olivine, while assuming a constant shear modulus throughout a planet (Table 2). We use radial temperature profiles for 100-Ma surfaces based on a conductive cooling model of a planet (Figure 4a). The interior temperature is assumed to be 1350°C, similar to that at the base of lithosphere on the Earth. Our planetary thermal structure may represent a reasonable estimate at shallow depths where heat conduction is the predominant heat transfer mechanism. As discussed in section 2.2, we assume a Newtonian rheology with $\eta_0 = 10^{19}$ Pa s in equation (8). The resulting viscosity based on a dry olivine rheology increases rapidly with decreasing depth (Figure 4b). As shown in Figure 4b, we impose a cutoff of 10^{30} Pa s at the shallow depth, but this cutoff does not affect the results as long as it is sufficiently large. For comparison, the effective elastic plate thickness for 100-Ma seafloor on Earth is about

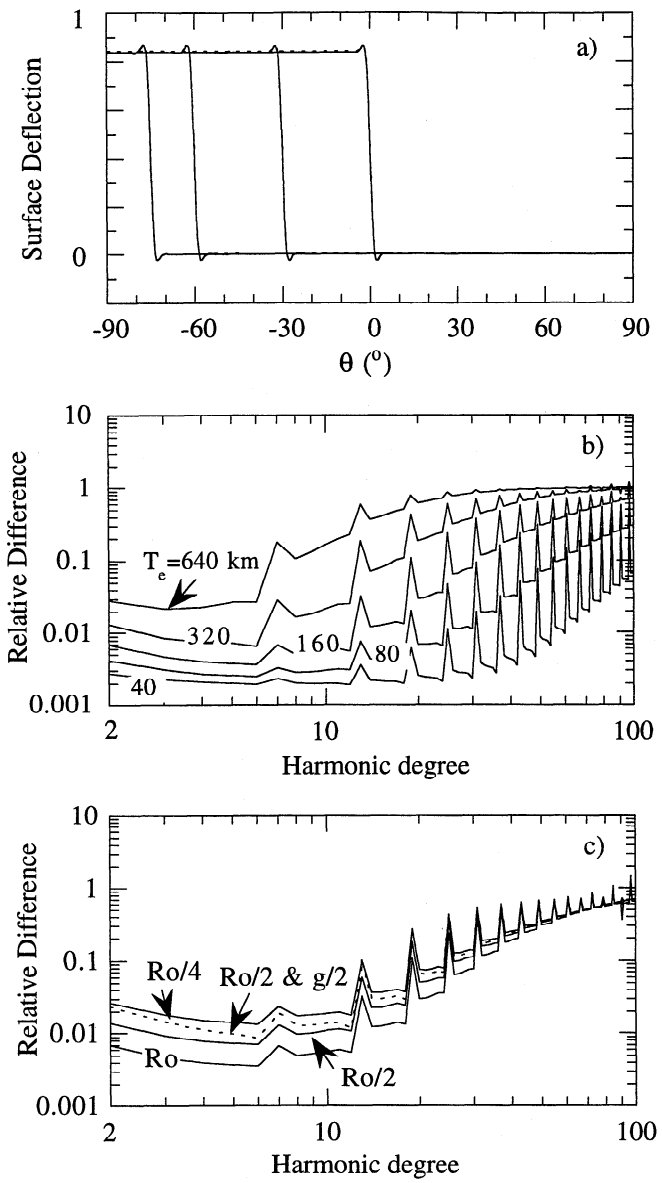

Figure 3. (a) Comparison of surface deflection in response to disk loads with different load radii from a thin elastic shell model (dashed lines) with the steady state surface deflection from a viscoelastic model (solid lines). The plot shows the relative difference in surface deflection at different harmonics between a thin elastic shell model and a viscoelastic model (i.e., steady state solution) (b) for different thicknesses for the top layer but with the same planetary radius; and (c) for different planetary radii but with the same ratio of the top layer thickness to planetary radius. The dashed line in Figure 3c is for a model with a planetary radius $R_0/2$ and a commensurately reduced gravitational acceleration.

40 km, based on the empirical relation between elastic plate thickness and surface age (or 550°C lithospheric temperature) [*McNutt,* 1984]. Figure 5a shows D_c at different spherical harmonics after 10^9 years loading for these three cases (we will defer discussions on the time evolution of crustal compensation to the next section on basin relaxation). It is clear that the compensation is strongly influenced by the planetary radius. While D_c is about 0.9 for a planetary radius of 6000 km, it decreases rapidly with decreasing radius.

Next we consider the Moon, Mars, and Earth with self-gravitation. Again, we assume a 100-Ma surface, but for the Earth and Mars we assume a wet olivine rheology. Model parameters are given in Table 2. For the case of the Moon, Figure 5b shows that surface loads 10^9 years subsequent to loading still deviate significantly from isostatic compensation, even if the surface (lithosphere) is as young as 100 Ma when the loads are initially applied. The value of D_c is only 0.18 at degree 2. For Mars we also observe significant deviation from isostatic compensation. For the Earth, D_c at degree 2 is about 0.98 and is close to 1 at other degrees as well (Figure 5b). This indicates that surface loads on the Earth are approximately compensated, as evident from the lack of correlation between the continents and the geoid anomalies.

As for degree of compensation, the Love numbers for viscoelastic models are time-dependent. The load Love number $k_L(l, t)$ are –1 and 0, respectively for for completely fluid and rigid planets [*Munk and MacDonald,* 1960]. The Love numbers for the Moon, Mars, and Earth at times corresponding to those in Figure 5b show that smaller planets with the same surface age appear to be more rigid, with Love numbers that differ significantly from –1 (Figure 5c). For example, for degree 2, while the Love number is –0.992 for the Earth, it is only -0.56 for the Moon and -0.96 for Mars.

3.3. Viscoelastic Relaxation of Lunar Basins

We now consider the general characteristics of stress relaxation and crustal compensation for lunar basins. We

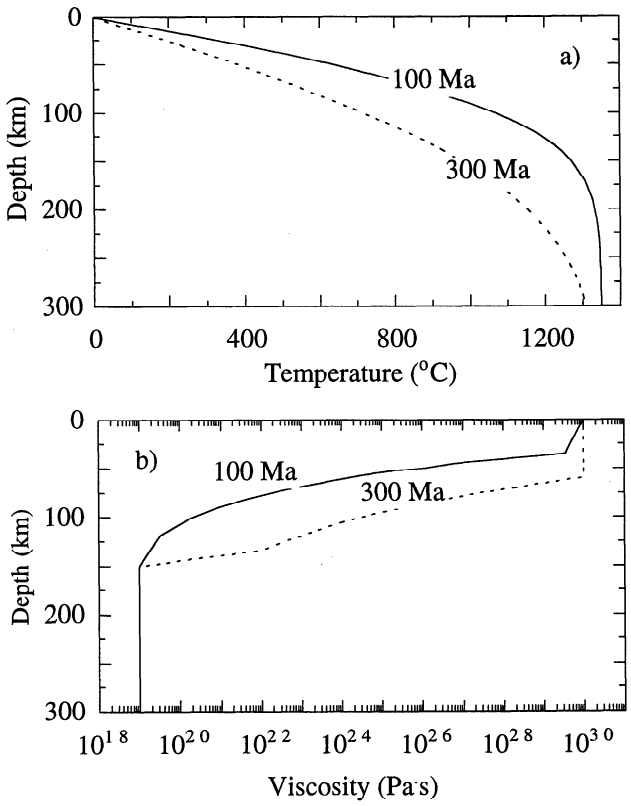

Figure 4. (a) Depth dependence of temperature for planets with 100-Ma and 300-Ma surfaces, assuming that heat conduction is the dominant heat transfer mechanism near the surface. (b) Depth dependence of viscosity estimated from the thermal structure in Figure 4a and a dry olivine rheology. Below a depth of 150 km the viscosity is assumed to be 10^{19} Pa s.

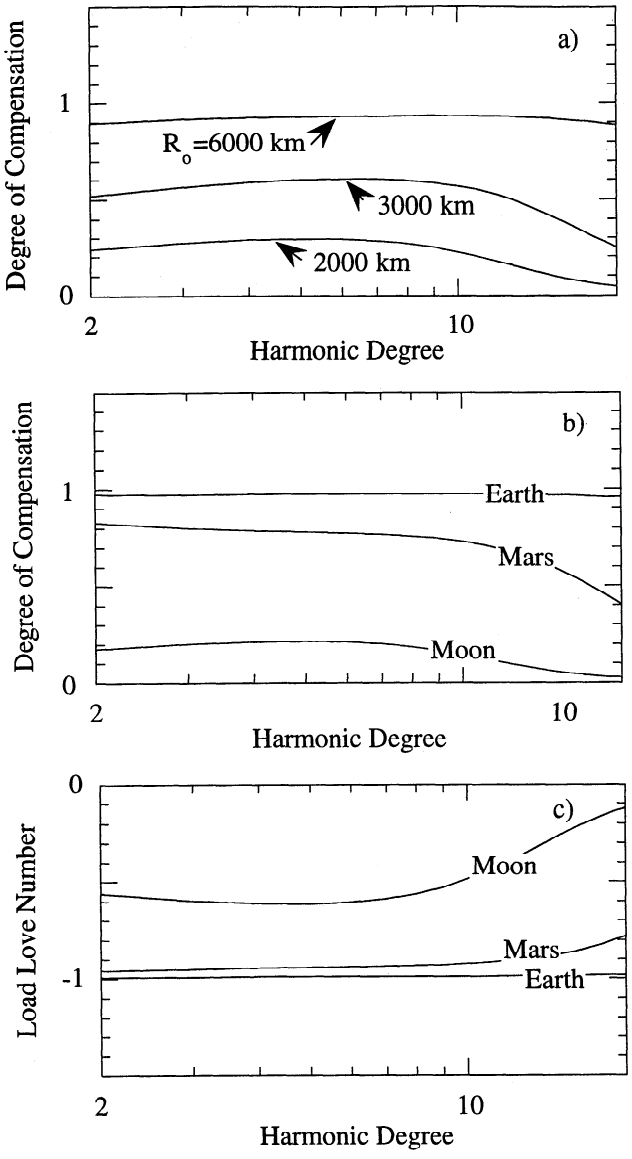

Figure 5. (a and b) Degree of compensation at different harmonic degrees 1 b.y. after loading on an initially 100-Ma planetary surface for planets with a uniform density and radii of 2000 km, 3000 km, and 6000 km radii (Figure 5a) and for the Moon, Mars, and Earth (Figure 5b), and (c) corresponding load Love numbers.

ignore self-gravitation because the predominant wavelengths of lunar basins are smaller than degree 6 (the self-gravitation is only important for the longest wavelengths). The gravitational acceleration is 1.63 m s^{-2} at the surface and decreases linearly with the depth, as expected for a planet with a constant density. In this analysis we do not assume laterally variable mechanical properties, though we recognize that impact-related weakening of the lithosphere may be an important effect that should be considered in future (numerical) studies.

When impact basins including the South Pole-Aitken basin (t >4 b.y.) and the Imbrium basin (t ~3.9 b.y.) were formed, the lunar surface was relatively young. Therefore in deriving the radial viscosity profile, we may use radial temperature profiles that are adequate for relatively young surfaces. We use radial temperature profiles for 100-Ma and 300-Ma surfaces (Figure 4a). Admittedly, these estimated temperature and viscosity profiles have large uncertainties, and in fact may be quite different in the vicinity of major impacts. Thus our results are most relevant to the time evolution of basin topography once a postimpact steady state thermal structure has been achieved. Future efforts will focus on models to account for impact-related heterogeneity in mechanical structure [*Zhong and Zuber,* 1999].

We investigate the case of a basin-shaped load with a radius of 30° (comparable with that for the South Pole-Aitken basin) and an initially unit depth on 100-Ma surfaces. Both the basin surface and Moho uplift in response to the load. Because the mantle viscosity is relatively small (Figure 4b), during the

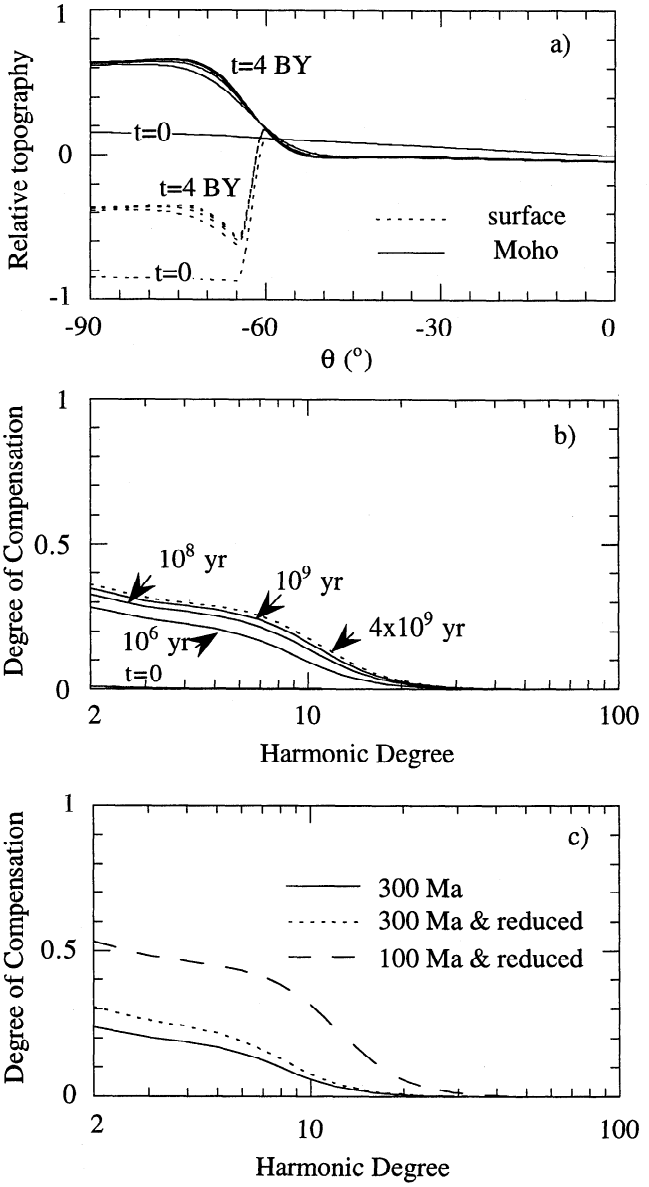

Figure 6. (a) Time evolution of surface and Moho topography. (b) Time evolution of degree of compensation for 100-Ma lunar surfaces in response to a basin-type topographic load. (c) Degree of compensation 1 b.y. after loading on an initially 300-Ma surface, and 100-Ma and 300-Ma surfaces with crustal viscosity reduced by a factor of 100 compared to that of the lithospheric mantle.

first 10^4 years the stresses within the mantle relax quickly, resulting in rapid uplift (Figure 6a). Uplift becomes progressively slower when stress relaxation begins to influence shallow depths where the viscosity is large. Figure 6a shows that distinct basin topography can be maintained through lunar geological history (> 4 b.y.). The degree of compensation is <0.4 for all harmonics, including degree 2, even 4 b.y. beyond the time of basin formation (Figure 6b). The basin thus never achieves a fully isostatic state; the deviation from isostasy is greater if the surface age is 300 Ma (Figure 6c), because of the overall higher viscosity (Figure 4b). For the above two calculations, we have also considered a reduced viscosity (by a factor of 100) for the crust, and the state of crustal compensation does not change significantly (Figure 6c). The strong core of the viscoelastic lithosphere still relaxes at rate controlled by its viscosity.

The parameter D_c depends only on the planetary viscoelastic properties and is independent of the load size [e.g., *Zhong,* 1997]. Therefore the dependence of D_c on harmonic degree (Figure 6b) suggests that lunar basins that formed in a laterally homogeneous lunar lithosphere should not be isostatically compensated, irrespective of their size. This result holds even if the interior of the Moon at the time of basin formation was relatively hot and high viscosity existed only at relatively shallow depths (Figure 4). While detailed modeling of the compensation states of lunar basins is beyond the scope of the present study, we note that recent geophysical data on lunar basins are indeed consistent with the expected deviation of these structures from the isostatic state. Except for the South Pole-Aitken basin, lunar basins exhibit large free-air gravity anomalies that indicate a deviation from compensation [*Zuber et al.,* 1994]. In fact, gravity/topography studies indicate a superisostatic state for some lunar basins prior to mare loading [*Neumann et al.,* 1996; *Konopliv et al.,* 1998], which requires that surface and subsurface relief of some premare basins was at least partially supported by the strength of the young lunar lithosphere. The nearly compensated South Pole-Aitken basin represents a special case that requires other compensation mechanisms.

3.4. Discussion

The dependence of degree of compensation on planetary radius was first suggested by *Turcotte et al.* [1981] and *Willemann and Turcotte* [1981] as effects of membrane stresses with their thin elastic shell models. Our viscoelastic models confirm and extend their results. As indicated by *Turcotte et al.* [1981], gravity anomalies on small planets are expected to be partially supported by the elastic lithosphere. Therefore the gravity anomalies should correlate with surface topography, as is generally (but not fully) consistent with observations on the Moon and Mars. At least two other factors may contribute to this correlation between topography and gravity. First, smaller planets have less capability to retain heat, and this tends to produce a thicker surface thermal boundary layer (i.e., thermal lithosphere). A thick thermal boundary layer has a great capacity to support surface topography (Figure 6c). Second, for small planets the greater capability of surface layers to support stresses also implies greater filtering effects of the surface layers on any gravity anomalies that may be produced by planetary mantle convection. Therefore in determining gravity anomalies associated with dynamic topography produced by mantle convection, these filtering effects should be considered, particularly for planets with relatively thick thermal boundary layers.

While the thin elastic shell models ignore radial stress variations, our viscoelastic models represent a complete description of stress relaxation. The comparisons between these two different models show that the elastic shell models represent a special case of a viscoelastic model in which the top layer is infinitely more viscous than the bottom layer. They also show that the thin elastic shell models provide a good description of the planetary response to surface loading if (1) T_e/R_o is relatively small, (2) R_o is relatively large, and (3) planetary internal mechanical structure can be described to first order as a two-layer structure. For the case of the Moon with $T_e = 80$ km, the thin elastic shell model could introduce greater than 10% error at all the wavelengths because of that body's relatively small radius and gravitational acceleration (Figures 3b and 3c).

It has long been recognized that the topographic flattening of the Moon is significantly greater than that of the gravity field. The greater topographic flattening has been proposed to be a consequence of the "memory" of an earlier Moon that was rotating faster and had a correspondingly larger hydrostatic flattening [*Jeffreys,* 1970; *Lambeck and Pullan,* 1980; *Willemann and Turcotte,* 1981]. Recent analysis [*Smith and Zuber,* 1998] has shown that other degree 2 terms of the lunar topographic field [*Smith et al.,* 1997] also significantly exceed their counterparts in the gravity field [*Konopliv et al.,* 1998], and are mutually consistent with a lunar rotation rate about 15 times greater than at present. Assuming synchronous rotation, the degree 2 topography would require that the Moon "froze in" its long-wavelength shape at a distance of 13 to 16 Earth radii. Such a scenario is problematic given dynamical studies [e.g., *Goldreich,* 1966] of the evolution of the Earth-Moon system that suggest that the Moon, which had a mostly molten exterior early in its history [*Wood et al.,* 1970], receded from Earth rapidly, before significant freezing out of the magma ocean likely occurred. Dynamical mechanisms that could slow the retreat of the Moon from Earth could cause significant heating of the lunar interior [*Touma and Wisdom,* 1994] and would exacerbate the problem of how to cool the Moon quickly enough to explain the degree 2 shape in the context of an earlier faster rotation. While the present analysis does not solve the problem, it does indicate that a body the size of the Moon would be expected to support degree 2 topography even if the lithospheric shell is relatively thin, thus requiring less cooling than would previously have been thought. Further modeling will be required to resolve the inconsistency.

Our results show that if the rheology of the lunar mantle can be approximated with dry olivine, then lunar basins which formed on relatively young surfaces (i.e., ~100-300 Ma) with thin lithospheres will not be compensated over the age of the Moon. This conclusion holds even with a moderately reduced viscosity in the crust. Many large lunar basins with mare basalt fill are not compensated [*Neumann et al.,* 1996]. The age of these mare basalts is generally around 3.9 b.y., while the basins are slightly older. Therefore these observations are in agreement with our model predictions. It is important to realize that in our models the lunar interior is relatively hot with a relatively low viscosity (Figure 4). Therefore the large viscosity for the lunar interiors as estimated by *Arkani-Hamad* [1973a] to support the lunar basins is not required. The large

viscosity estimate by *Arkani-Hamad* [1973a] is mainly due to the inadequate constant viscosity assumption used in his relaxation model.

The South Pole-Aitken basin is the oldest, largest (2200 km diameter), and deepest basin on the Moon, with its age as old as the crust age on the farside (> 4 b.y.), its radius of about 30°, and its depth of about 8 km [*Spudis et al.*, 1994; *Zuber et al.*, 1994]. South Pole-Aitken does not contain significant mare basalt fill [*Lucey et al.*, 1996] and is nearly compensated [*Zuber et al.*, 1994; *Neumann et al.*, 1996; *Konopliv et al.*, 1998]. Apparently, to explain the compensation, the lunar surface is required to have been extremely young when the SP-Aitken basin was formed. However, extremely young surfaces that would be consistent with compensation may not explain how the distinct basin topography (i.e., ~8 km deep) had been maintained during the compensation process; weak crust and lithosphere may facilitate crustal channel flow and therefore may not be capable of supporting topographic anomalies [*Bird*, 1991; *Zhong*, 1997]. We believe that the compensation of the SP-Aitken basin is likely a consequence of lateral variations in thermal and mechanical structure caused by the impact process. Lateral variations in structure have not been considered in our models, due to the limitations of our analytic solution techniques, but efforts are under way to account for such effects. We also expect that such effects would contribute to the compensation of other major lunar impact basins, and, in fact, one might intuitively expect that weakening of the lithosphere in the vicinity of major basins would result in a state of isostasy prior to mare flooding [*Bratt et al.*, 1985a, b]. However, the observed deviation of isostasy of most basins indicates that thermal and mechanical weakening were not adequate to permit complete relaxation of stresses associated with basin formation. This observation justifies to first order our assumption of a laterally homogeneous lithosphere.

4. Conclusions

We have formulated a stress relaxation model for self-gravitating planets with a multilayer linear viscoelastic rheology. We have applied this model to study the evolution of crustal compensation on the terrestrial planets and basin relaxation on the Moon. We have demonstrated that the thin elastic shell models [*Brotchie and Silvester*, 1969; *Brotchie*, 1971; *Turcotte et al.*, 1981] represent a special case of viscoelastic model that includes two viscosity layers with an infinitely large viscosity contrast. This representation is accurate to within 5% as long as the wavelengths are 5 times greater than the elastic plate thickness and the shell radius is relatively large.

With the assumptions that lunar rheology can be represented with dry olivine and that the shallow thermal structure can be approximated with a simple conductive cooling model, we find that lunar basins will not achieve compensation throughout the lunar geological history, even if the surfaces on which the basins were initially formed were relatively young (i.e., 100 – 300 Ma). For 100-Ma surfaces the degree of compensation is less than 0.3, and load Love numbers are greater than -0.6 for all the harmonics including degree 2 even after 10^9 years relaxation. This conclusion does not change significantly even with a moderately reduced viscosity for the crust. If a similar viscosity structure (i.e., derived from a 100-Ma surface) is assumed for Earth, the crust will become largely compensated with degree of compensation and load Love number at degree 2 that are about 0.97 and −0.99 after 10^7, respectively, close to those for a purely fluid Earth model. These results indicate that crustal compensation is strongly dependent on planetary radius, consistent with the proposal by *Turcotte et al.* [1981] that membrane stress can support significant long-wavelength gravity anomalies. The tendency for a small body like the Moon to support long-wavelength stresses may be relevant in understanding the degree 2 terms in the lunar shape in the context of a fossil tidal bulge.

The fact that the South Pole-Aitken basin is largely compensated indicates that lateral variations in thermal or/and mechanical structure induced by impact processes likely also play a significant role in crustal compensation. The nearly 1% difference in the Love number at degree 2 between the purely fluid Earth model and the model with a strong surface layer (i.e., equivalent to the rheology for 100-Ma surfaces) may have important implications with regard to true polar wander for the Earth [e.g., *Kirschvink et al.*, 1997]. However, the Earth's surface also has significant lateral variations in mechanical strength due to effects such as faulted and presumably weak plate margins and different surface ages. Such variations in thermal and mechanical structure should be included in future studies.

Appendix A: Nondimensionalization and Laplace Transform of the Governing Equations

We may nondimensionalize equations (1)-(4) with

$$\sigma_{ij}' = \frac{\sigma_{ij}}{\mu_0}, \quad t' = \frac{t}{\eta_0/\mu_0}, \quad x_i' = \frac{x_i}{R_o}, \quad \phi' = \frac{\phi}{4\pi G \rho_r R_o^2},$$

$$\mu' = \frac{\mu}{\mu_0}, \quad \eta' = \frac{\eta}{\eta_0}, \quad \rho_0' = \frac{\rho_0}{\rho_r}, \quad \Delta\rho' = \frac{\Delta\rho}{\rho_r}, \tag{A1}$$

where R_0 is the outer radius of the planet; and ρ_r, μ_0, and η_0 are the constant reference density, shear modulus, and viscosity, respectively. After dropping the primes, the resulting equations are

$$u_{i,i} = 0, \tag{A2}$$

$$(\sigma_{ij} + R_{sg}\rho_0\phi\delta_{ij})_{,j} - R_b\Delta\rho\delta_{ir} = 0, \tag{A3}$$

$$\phi_{,ii} = \Delta\rho, \tag{A4}$$

$$\sigma_{ij} + \tau\dot{\sigma}_{ij} = -P\delta_{ij} + 2\eta\dot{\varepsilon}_{ij}, \tag{A5}$$

where $R_{sg} = 4\pi G\rho_r^2 R_0^2/\mu_0$, $R_b = \rho_r g R_0/\mu_0$, $\tau = \eta/\mu$.

After performing a Laplace transform on equations (A2)–(A5), the mathematical forms of the resulting equations in a Laplacian space do not change, except equation (A5), which becomes

$$\sigma_{ij} = -p\delta_{ij} + 2\eta(s)\dot{\varepsilon}_{ij}, \tag{A6}$$

where $\eta(s) = \eta/(1+s\tau)$. In performing the Laplace transform on (A5), the initial stresses are assumed to be zero.

Appendix B: Dependence of Gravitational Potential and Radial Stress on Topography

Prior to introducing the solution approach, it is desirable to derive the relationships between topography, radial stress, and the perturbation of gravitational potentials. We first consider the kinematic conditions in a time domain,

$$V_r(t)=\frac{dF(t)}{dt}. \tag{B1}$$

Assume that at t=0, the values of initial relief at a given harmonic degree l and at density interfaces corresponding to the surface (r_s), crust-mantle boundary (r_m), and the core-mantle boundary (r_b) are F_{s0}, F_{m0}, and 0, respectively. We perform the Laplace transform on the kinematic conditions,

$$V_r(r_s,s)=sF_s-F_{s0}, \tag{B2}$$

$$V_r(r_m,s)=sF_m-F_{m0}, \tag{B3}$$

$$V_r(r_b,s)=sF_b. \tag{B4}$$

Now we may consider the relationship between the perturbation of gravitational potential and the relief at the density interfaces, which is essentially the solution of Poisson's equation. We may write

$$\phi_b=\frac{1}{2l+1}\left[r_b^l\Delta\rho_s F_s+r_m\left(\frac{r_b}{r_m}\right)^l\Delta\rho_m F_m+r_b\Delta\rho_b F_b\right], \tag{B5}$$

$$\phi_m=\frac{1}{2l+1}\left[r_m^l\Delta\rho_s F_s+r_m\Delta\rho_m F_m+r_b\left(\frac{r_b}{r_m}\right)^{l+1}\Delta\rho_b F_b\right], \tag{B6}$$

and

$$\phi_s=\frac{1}{2l+1}[\Delta\rho_s F_s+r_m^{l+2}\Delta\rho_m F_m+r_b^{l+2}\Delta\rho_b F_b], \tag{B7}$$

where ϕ_i and $\Delta\rho_i$ for i=s, m, and b are the perturbation of gravitational potential and density contrast (positive) at these three density interfaces.

For a self-gravitating planet, with a linear approximation, the relief at the surface and bottom interfaces can be related to σ_{rr} at these boundaries as

$$\sigma_{rr}(r_s)=-R_b\Delta\rho_s F_s, \tag{B8}$$

$$\sigma_{rr}(r_b)+\rho_m R_{sg}\phi_b=R_b\Delta\rho_b F_b-\Delta\rho_b R_{sg}\phi_b, \tag{B9}$$

where the inviscid core is also assumed to be self-gravitating [e.g., *Zhang and Christensen,* 1993].

Appendix C: Propagator Matrix Solutions for Eigenvalue Problems

With the above relationships it is now appropriate to introduce the solution approaches. In a spherical geometry, we define

$$\nu=\ln(r),\ V_r=y_1Y_{lm},\ V_\theta=y_2Y_{lm}^\theta,\ V_\varphi=y_2Y_{lm}^\varphi,$$

$$\sigma_{rr}=y_3Y_{lm},\ \sigma_{r\theta}=y_4Y_{lm}^\theta,\ \sigma_{r\varphi}=y_4Y_{lm}^\varphi,\ \Delta\rho=y_8Y_{lm}, \tag{C1}$$

where Y_{lm} is the normalized spherical harmonic function [e.g., *Arfken,* 1970],

$$Y_{lm}=P_{lm}(\cos(\theta))\begin{bmatrix}\cos(m\varphi)\\ \sin(m\varphi)\end{bmatrix}, \tag{C2}$$

$$Y_{lm}^\theta=\frac{\partial Y_{lm}}{\partial\theta},\quad Y_{lm}^\varphi=\frac{1}{\sin(\theta)}\frac{\partial Y_{lm}}{\partial\varphi}. \tag{C3}$$

By further defining $\vec{u}(s)=[u_1,u_2,u_3,u_4]^T=[y_1,y_2,r(y_3+R_{sg}\rho_0\phi),ry_4]^T$, the governing equations can be written as

$$\frac{d\vec{u}(s)}{d\nu}=A(s)\vec{u}(s)+\vec{b}(s), \tag{C4}$$

where

$$A(s)=\begin{bmatrix}-2 & L & 0 & 0\\ -1 & 1 & 0 & 1/\eta(s)\\ 12\eta(s) & -6L\eta(s) & 1 & L\\ -6\eta(s) & 2(2L-1)\eta(s) & -1 & -2\end{bmatrix}, \tag{C5}$$

$$\vec{b}(s)=\begin{bmatrix}0, & 0, & r^2R_by_8, & 0\end{bmatrix}^T, \tag{C6}$$

and $L=l(l+1)$. It can be shown that the Laplace variable s in $A(s)$ does not affect its eigenvalues $l+1$, $-l$, $l-1$, and $-l-2$. We next define a propagator matrix (a function of s) as

$$P(\nu,\nu_0)=\sum_{k=1}^{4}\left\{\exp[\lambda_k(\nu-\nu_0)]\frac{\prod_{i\neq k}[A(s)-\lambda_i I]}{\prod_{i\neq k}[\lambda_k-\lambda_i]}\right\}. \tag{C7}$$

Then the solution of $\vec{u}(\nu_2)$ can be related to $\vec{u}(\nu_1)$ as

$$\vec{u}(\nu_2)=P(\nu_2,\nu_1)\vec{u}(\nu_1)+\int_{\nu_1}^{\nu_2}P(\nu_2,\xi)b(\xi)d\xi, \tag{C8}$$

where ν_1 and ν_2 are located within a layer with homogeneous viscoelastic properties.

For a multiple-layer viscoelastic structure, we shall consider only the buoyancy forces associated with topographic variations at the three density interfaces (surface, crust-mantle boundary, and the core-mantle boundary) whose radial coordinates are ν_s, ν_m, and ν_0, respectively. Then the solution of $\vec{u}(\nu)$ can be related to $\vec{u}(\nu_0)$ at the core-mantle boundary as

$$\vec{u}(\nu_m)=M\vec{u}(\nu_0)=P_m(\nu_m,\nu_{m-1})P_{m-1}(\nu_{m-1},\nu_{m-2})\cdots P_1(\nu_1,\nu_0)\vec{u}(\nu_0), \tag{C9}$$

$$\vec{u}(\nu_s)=S\vec{u}(\nu_0)+C\vec{J}_m=P_s(\nu_s,\nu_{s-1})P_{s-1}(\nu_{s-1},\nu_{s-2})\cdots P_1(\nu_1,\nu_0)\vec{u}(\nu_0)+P_s(\nu_s,\nu_{s-1})\cdots P_{m+1}(\nu_{m+1},\nu_m)\vec{J}_m \tag{C10}$$

where M, S, and C are the matrices depending on the Laplace variable s; the subscripts m and s are the layer indices, and $\vec{J}_m=[0,\ 0,\ r_m\Delta\rho_m(R_bF_m-R_{sg}\phi_m),\ 0]^T$ results from a jump in normal stresses at the crust-mantle boundary.

From the first equation of (C9) we see that

$$-F_{m0}+sF_m=M_{11}sF_b+M_{12}y_{2b}+M_{13}r_b\Delta\rho_b(R_bF_b-R_{sg}\phi_b), \tag{C11}$$

and from the first, third, and fourth equations of (C10) we may write

$$-F_{s0}+sF_s=S_{11}sF_b+S_{12}y_{2b}+S_{13}r_b\Delta\rho_b(R_bF_b-R_{sg}\phi_b)+C_{13}r_m\Delta\rho_m(R_bF_m-R_{sg}\phi_m), \quad \text{(C12)}$$

$$-r_s\Delta\rho_s[R_bF_s-R_{sg}\phi_s]=S_{31}sF_b+S_{32}y_{2b}+S_{33}r_b\Delta\rho_b(R_bF_b-R_{sg}\phi_b)+C_{33}r_m\Delta\rho_m(R_bF_m-R_{sg}\phi_m), \quad \text{(C13)}$$

$$0=S_{41}sF_b+S_{42}y_{2b}+S_{43}r_b\Delta\rho_b(R_bF_b-R_{sg}\phi_b)+C_{43}r_m\Delta\rho_m(R_bF_m-R_{sg}\phi_m). \quad \text{(C14)}$$

Substituting equations (B5)-(B7) into equations (C11)-(C14) leads to four equations for four unknowns F_b, F_m, F_s, and y_{2b} in Laplacian space. In matrix form, the system of equations (C11)-(C14) can be written as

$$K(s)U(s)=F(s), \quad \text{(C15)}$$

where $U(s)=[F_b(s),F_m(s),F_s(s),y_{2b}(s)]^T$. Symbolic solutions for these four unknowns in $U(s)$ can be obtained in a Laplace space by solving equation (C15), and the solutions can be transformed back to time domain with a reverse Laplace transform [*Zhong,* 1997]. While $F(s)$ includes all the driving force terms (i.e., the perturbed topography along each density interface), matrix $K(s)$ only depends on geometrical and mechanical parameters. The eigenvalue equation $\det[K(s)]=0$ can be solved for the eigenvalues that determine the timescale of stress relaxation. Therefore the relaxation timescale is only dependent on geometrical and mechanical properties of the model. Each viscosity interface introduces two relaxation modes, while each density interface results in one relaxation mode [*Han and Wahr,* 1995; *Fang and Hager,* 1995].

Acknowledgments. This research was supported by the NASA Planetary Geology and Geophysics Program. We would like to thank B. H. Hager for suggesting the calculation of the Love numbers and O. Aharonson, B. Banerdt, and M. Wieczorek for useful comments.

References

Arfken, G., *Mathematical Methods for Physicists,* 815 pp., Academic, San Diego, Calif. 1970.

Arkani-Hamad, J., Viscosity of the Moon, *Moon, 6,* 112-124, 1973a.

Arkani-Hamad, J., Stress differences in the Moon as an evidence for a cold Moon, *Moon, 6,* 135-163, 1973b.

Artyushkov, E. V., Stresses in the lithosphere due to crustal thickness heterogeneities, *J. Geophys. Res., 78,* 7675-7708, 1973.

Banerdt, W. B., Support of long-wavelength loads on Venus and implications for internal structure, *J. Geophys. Res., 91,* 403-419, 1986.

Banerdt, W. B., R. J. Phillips, N. H. Sleep, and R. S. Saunders, Thick shell tectonics one-plate planets: Applications to Mars, *J. Geophys. Res., 87,* 9723-9733, 1982.

Bird, P., Lateral extrusion of lower crust from under high topography in the isostatic limit, *J. Geophys. Res., 96,* 10,275-10,286, 1991.

Bratt, S. R., S. C. Solomon, and J. W. Head, The evolution of impact basins: Cooling, subsidence, and thermal stress, *J. Geophys. Res., 90,* 12,415-12,433, 1985a.

Bratt, S. R., S. C. Solomon, J. W. Head, and C. H. Thurber, The deep structure of lunar basins: Implications for basin formation and modification, *J. Geophys. Res., 90,* 3049-3064, 1985b.

Brotchie, J. F., Flexure of a liquid-filled spherical shell in a radial gravity field, *Mod. Geol., 3,* 15-23, 1971.

Brotchie, J. F., and R. Silvester, On crustal flexure, *J. Geophys. Res., 74,* 5240-5252, 1969.

Cathles, L. M., *The Viscosity of the Earth's Mantle,* 386 pp., Princeton Univ. Press, Princeton, N. J., 1975.

Comer, R. P., Thick plate flexure, *Geophys. J. R. Astron. Soc., 72,* 101-113, 1983.

Comer, R. P., S. C. Solomon, and J. W. Head, Mars: Thickness of the lithosphere from the tectonic response to volcanic loads, *Rev. Geophys., 23,* 61-92, 1985.

Dziewonski, A. M., and D. L. Anderson, Preliminary reference Earth model, *Phys. Earth Planet. Inter., 25,* 297-356, 1981.

Fang, M., and B. H. Hager, The singularity mystery associated with a radially continuous Maxwell viscoelastic structure, *Geophys. J. Int., 123,* 849-865, 1995.

Goldreich, P., History of the lunar orbit, *Rev. Geophys., 4,* 411-439, 1966.

Hager, B. H. and R. J. O'Connell, A simple global model of plate dynamics and mantle convection, *J. Geophys. Res., 86,* 4843-4867, 1981.

Hager, B. H., and M. A. Richards, Long-wavelength variations in Earth's geoid: Physical models and dynamical implications, *Philos. Trans. R. Soc. London, Ser. A, 328,* 309-327, 1989.

Han, D., and J. Wahr, The viscoelastic relaxation of a realistically stratified Earth and a further analysis of post-glacial rebound, *Geophys. J. Int., 120,* 287-311, 1995.

Janes, D. N., and H. J. Melosh, Tectonics of planetary loading: A general model and results, *J. Geophys. Res., 95,* 21,345-21,355, 1990.

Jeffreys, H., *The Earth,* 525 pp., Cambridge Univ. Press, New York, 1970.

Karato, S., and P. Wu, Rheology of the upper mantle: A synthesis, *Science, 260,* 771-778, 1993.

Kaula, W. M., *An Introduction to Planetary Physics: The Terrestrial Planets,* John Wiley, New York, 1968.

Kennett, B. L. N., S. Widiyantoro, and R. D. van der Hilst, Joint seismic tomography for bulk sound and shear wave speed in the Earth's mantle, *J. Geophys. Res., 103,* 12,469-12,493, 1998.

Kirschvink, J. L., R. L. Ripperdan, and D. A. Evans, Evidence for a large-scale reorganization of early Cambrian continental masses by inertial interchange true polar wander, *Science, 277,* 541-545, 1997.

Konopliv, A. S., A. Binder, L. Hood, A. Kucinskas, W. L. Sjogren, J. G. Williams, Gravity field of the Moon from Lunar Prospector, *Science, 281,* 1476-1480, 1998.

Kraus, H., *Thin Elastic Shells: An Introduction to the Theoretical Foundation and Analysis of Their Static and Dynamic Behavior,* 476 pp., John Wiley, New York, 1967.

Lambeck, K., *The Earth's Variable Rotation,* Cambridge Univ. Press, New York, 1980.

Lambeck, K., and S. Pullan, The lunar fossil bulge hypothesis revisited, *Phys. Earth. Planet. Inter., 22,* 12-28, 1980.

Lucey, P. G., P. D. Spudis, M. Zuber, D. Smith, and E. Malaret, Topographic-compositional units on the Moon and the early evolution of the lunar crust, *Science, 266,* 1855-1858, 1996.

McNutt, M. K., Lithospheric flexure and thermal anomalies, *J. Geophys. Res., 89,* 11,180-11,194, 1984.

Mitrovica, J., and A. M. Forte, Radial profile of mantle viscosity: Results from the joint inversion of convection and postglacial rebound observables, *J. Geophys. Res., 102,* 2751-2769, 1997.

Mitrovica, J. X., and W. R. Peltier, A comparison of methods for the inversion of viscoelastic relaxation spectra, *Geophys. J. Int., 108,* 410-414, 1992.

Muller, P.M., and W.L. Sjogren, Mascons: Lunar mass concentrations, *Science, 161,* 680-684, 1968.

Munk, W., and G. J. F. MacDonald, *The Rotation of the Earth,* 323 pp., Cambridge Univ. Press, New York, 1960.

Neumann, G. A., M. T. Zuber, D. E. Smith, and F. G. Lemoine, The lunar crust: Global signature and structure of major basins, *J. Geophys. Res., 101,* 16,841-16,863, 1996.

Peltier, W. R., The impulse response of a Maxwell Earth, *Rev. Geophys., 12,* 649-669, 1974.

Peltier, W. R., Glacial isostatic adjustment, II, The inverse problem, *Geophys. J. R. Astron. Soc., 46,* 605-646, 1976.

Phillips, R. J., and K. Lambeck, Gravity fields of the terrestrial planets: Long wavelength anomalies and tectonics, *Rev. Geophys., 18,* 27-86, 1980.

Ranalli, G., *Rheology of the Earth,* Chapman and Hall, New York, 1995.

Sleep, N. H., and R. J. Phillips, Gravity and lithospheric stress on the terrestrial planets with reference to the Tharsis region on Mars, *J. Geophys. Res., 90,* 4469-4489, 1985.

Smith, D. E., and M. T. Zuber, Inferences about the early Moon from

gravity and topography, paper presented at Conference on the Origin of the Earth and Moon, Lunar and Planet. Inst., Monterrey, Calif., 1998.

Smith, D. E., M. T. Zuber, G. A. Neumann, and F. G. Lemoine, Topography of the Moon from the Clementine LIDAR, *J. Geophys. Res., 102,* 1591-1611, 1997.

Solomon, S. C., and J. W. Head, Vertical movements in mare basins: Relation to mare emplacement, basin tectonics, and lunar thermal history, *J. Geophys. Res., 84,* 1667-1682, 1979.

Spudis, P. D., R. A. Riesse, and J. G. Gillis, Ancient multiring basins on the Moon revealed by Clementine laser altimetry, *Science, 266,* 1848-1851, 1994.

Su, W.-J., and A .M. Dziewonski, Simultaneous inversion for 3D variations in shear and bulk velocity in the mantle, *Phys. Earth Planet. Inter., 100,* 135-156, 1996.

Toksoz, M. N., A. M. Dainty, S. C. Solomon, and K. R. Anderson, Structure of the Moon, *Rev. Geophys., 12,* 539-567, 1974.

Touma, J., and J. Wisdom, Evolution of the Earth-Moon system, *Astron. J., 108,* 1943-1961, 1994.

Turcotte, D. L., A fractal interpretation of topography and geoid spectra on the Earth, Moon, Venus, and Mars, *Proc. Lunar Planet. Sci. Conf.,* 17th Part 2, *J. Geophys. Res., 92,* suppl., E597-E601, 1987.

Turcotte, D. L., and G. Schubert, *Geodynamics,* John Wiley, New York, 1982.

Turcotte, D. L., R. J. Willemann, W. F. Haxby, and J. Norberry, Role of membrane stresses in the support of planetary topography, *J. Geophys. Res., 86,* 3951-3959, 1981.

Willemann, R. J. and D. L. Turcotte, Support of topographic and other loads on the Moon and on the terrestrial planets, *Proc. Lunar Planet. Sci., 12th,* 837-851, 1981.

Wood, J.A., J.S. Dickey, Jr., U.B. Marvin, and B.N. Powell, Lunar anorthosites and a geophysical model for the Moon, *Proc. Apollo 11 Lunar Sci. Conf., 1,* 958-988, 1970.

Zhang, S., and U. R. Christensen, Some effects of lateral viscosity variations on geoid and surface velocities induced by density anomalies in the mantle, *Geophys. J. Int., 114,* 531-547, 1993.

Zhong, S., Dynamics of crustal compensation and its influences on crustal isostasy, *J. Geophys. Res., 102,* 15,287-15,299, 1997.

Zhong, S., and M. T. Zuber, Stress relaxation for axisymmetric planets with lateral variations in viscoelastic properties and its implications to compensation of lunar basins, *Eos Trans. Am. Geophys. Un., 80,* No. 17, 208, Suppl., 1999.

Zuber, M. T., D. E. Smith, F. G. Lemoine, and G. A. Neumann, The shape and internal structure of the Moon from the Clementine mission, *Science, 266,* 1839-1843, 1994.

S. Zhong and M. T. Zuber, Department of Earth, Atmospheric, and Planetary Sciences, Massachusetts Institute of Technology, Cambridge, MA 02139. (e-mail: szhong@rayleigh.mit.edu)

(Received April 27, 1999; revised October 27, 1999;
accepted November 1, 1999.)